

Analytic Study of Three-Dimensional Single Cell Migration with and without Proteolytic Enzymes

REBECCA H. CHISHOLM,¹ BARRY D. HUGHES,¹ KERRY A. LANDMAN,¹ and MUHAMMAD H. ZAMAN²

¹Department of Mathematics and Statistics, University of Melbourne, Victoria 3010, Australia;
and ²Department of Biomedical Engineering, Boston University, Boston, MA 02118, USA

(Received 12 May 2012; accepted 22 November 2012; published online 18 December 2012)

Associate Editor Paul Janmey oversaw the review of this article.

Abstract—Cell motility is a fundamental physiological process that regulates cellular fate in healthy and diseased systems. Cells cultured in 3D environments often exhibit biphasic dependence of migration speed with cell adhesion. Much is not understood about this very common behavior. A phenomenological model for 3D single-cell migration that exhibits biphasic behavior and highlights the important role of steric hindrance is developed and studied analytically. Changes in the biphasic behavior in the presence of proteolytic enzymes are investigated. Our methods produce a framework to determine analytic formulae for the mean cell speed, allowing general statements in terms of parameters to be explored, which will be useful when interpreting future experimental results. Our formula for mean cell speed as a function of ligand concentration generalizes and extends previous computational models that have shown good agreement with *in vitro* experiments.

Keywords—Cell migration, ECM, Biphasic speed, MMPs.

INTRODUCTION

Cell migration is a fundamental physiological process exhibited by nearly all cells *in vitro* and *in vivo*. Cell migration plays an important role in many biological processes and none more so than during tumour metastasis where single cells and clusters of cells undergo epithelial mesenchymal transition (EMT) and move away from the main tumour to establish secondary tumours in other parts of the body.²⁸ Therefore, understanding single-cell and collective cell migration is an important area of study.

Early experiments and models have focused on single cell migration *in vitro* in 2D environments.^{8,9,16,19,20,23} More recent work, and perhaps more relevant, has been

on understanding cell migration *in vitro* in 3D and *in vivo* environments.^{6,12,22,25,27,37,38} Migration of a cell *in vivo* (3D migration) requires the cell not just to move across a substratum (2D migration), but to navigate its way through extracellular matrix (ECM) which can have pore sizes comparable to or smaller than the diameter of a cell. Therefore the issue of steric hindrance seems to be important in any model of three-dimensional cell motility *in vivo*.

The most commonly used metric to quantify cellular motion is the speed of a cell tracked over time. The speed of a cell migrating through a complex environment is highly dependent on how the cell adapts to and interacts with its complex surroundings. Key factors involved in *in vivo* migration include interactions between a cell and the matrix (through receptors called integrins) and the ability of cells to overcome steric resistance using proteolytic enzymes (the largest class of which is the matrix metalloproteases (MMPs)).^{10,21}

Cell speed, as a function of density of available ligands or cell adhesion receptors, often exhibits a biphasic behavior:^{22,27,38} cells cultured across different adhesive environments display speeds that are low for low adhesion (ligand concentration), increase as adhesion increases, attain a maximum, and then decrease as adhesion increases further. While experimental and computational studies have addressed some key aspects of cellular motion in 2D and 3D environments,^{7,12,20,22,27,37,38} a number of fundamental questions remain unanswered. How do MMPs and steric hindrances affect the ability of a cell to achieve biphasic speed? Is cell migration inherently biphasic? Is the maximum cell speed higher if the cell can produce MMPs or is the maximum speed achieved at lower or higher ligand concentrations?

We present a phenomenological model of a cell moving through a 3D environment, over a single time-averaged cell motility cycle involving protrusion, adhesion and detachment. Although the model is

Address correspondence to Muhammad H. Zaman, Department of Biomedical Engineering, Boston University, Boston, MA 02118, USA. Electronic mail: rhc@ms.unimelb.edu.au, barrydh@unimelb.edu.au, kerry@unimelb.edu.au, zaman@bu.edu

phenomenological, it represents key physical mechanisms in a quantifiable way. The model can be investigated analytically, in the sense that its predictions can be extracted without recourse to simulation. Furthermore, as relevant future experimental evidence emerges, it will be possible to adjust the simple but natural functional relationships on which the model is based to match more closely biological data.

By considering the force balance over the cycle,^{5,12,33,34,37} we determine the velocity of a cell as a function of the ECM ligand density, consistent with experimental data.^{22,27,38} To study our model systematically, MMP activity is at first ignored; an extended version of the model then includes MMP activity and its effect on the forces on the cell. Changes in the nature of the biphasic behavior of the cell are investigated in the presence of MMPs. Our methods produce a framework for deriving an analytic formula for the mean cell speed, allowing general statements in terms of parameters to be explored and assisting in the interpreting of future experimental results.

In contrast, previous work^{5,12,33,34,37} was confined to numerical simulations, for specific parameter values. We compare our analytical model to the results of simulation methods where cell migration speed is tracked over time in a degrading environment, where the ECM properties are given as functions of time. We show that our analytical formulae for mean cell speed as a function of ligand concentration matches the results of the simulated data from this computational model. Consequently, our analytic approach generalizes and extends previous computational models that have shown good agreement with *in vitro* experiments, enables all parameter regimes to be explored, and allows general conclusions to be drawn.

MODEL FORMULATION FOR SINGLE CELL MOTILITY

A phenomenological model of a cell moving through a 3D environment, over a single time-averaged cell motility cycle involving protrusion, adhesion and detachment is considered here. The environment is made up of ECM, which contains binding ligands. A cell moving in such an environment has cell receptors (integrins) on the cell membrane, which allow the receptor and ligand to bind, allowing the cell to move in the 3D environment (Fig. 1).

We assume that a cell migrating in an ECM with a concentration L of binding ligands, is in mechanical equilibrium and the forces acting on a cell during one protrusion, adhesion and detachment cycle determine the cell's velocity $\mathbf{v}(L)$ during that cycle and are governed by the force balance equation

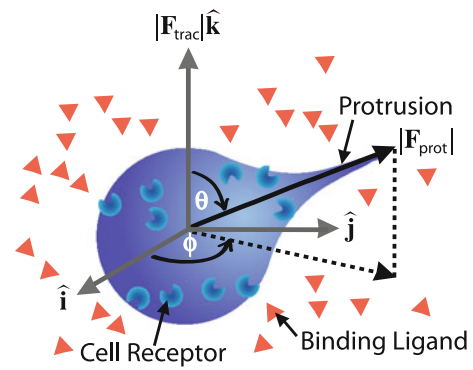


FIGURE 1. Schematic representation of the cell showing ligands, receptors, forces and coordinate system.

$$\mathbf{F}_{\text{total}} = \mathbf{F}_{\text{prot}} + \mathbf{F}_{\text{trac}} + \mathbf{F}_{\text{drag}} = \mathbf{0}. \quad (1)$$

During the cycle, none of the three forces that contribute to the total force will be precisely constant and the equation of motion is interpreted here as having been averaged over the cycle.

We assume that the cell has a fixed number of receptors $N = n_f + n_b$ and that the cell is polarized, so that its surface receptors are asymmetrically distributed between front (n_f) and the back (n_b) of the cell, where by definition $n_f > n_b$. Starting from a random direction, the cell randomly chooses a direction to protrude, in the absence of a chemical gradient. The force \mathbf{F}_{prot} arises from actin polymerization at the position of lamellipod extension, and as noted above, in our modeling approach its magnitude $F_{\text{prot}} = |\mathbf{F}_{\text{prot}}|$ is taken to be the time-averaged value over the whole cell motility cycle.

We assume that the drag force is proportional to the velocity, but the effective drag coefficient is affected both by normal fluid mechanical considerations and by structural properties of the ECM. We write

$$\mathbf{F}_{\text{drag}} = -cH(L)\mathbf{v}(L), \quad (2)$$

where $\mathbf{v}(L)$ is the velocity of a migrating cell, which depends on ECM ligand concentration L . The dimensioned factor c is intended to represent the constitutive response of the extracellular fluid. For comparison with previous simulation results in Fig. 5, we have assigned a value to c using the Stokes drag coefficient for a sphere of radius a in a Newtonian fluid of viscosity η , so that $c = 6\pi\eta a$, but neither this identification of the nature of the constitutive response nor the assumption of spherical geometry is a necessary physical assumption in the model.

The dimensionless factor $H(L)$, which we take to be an increasing function of ligand concentration L , will

be referred to as *steric hindrance*.¹² This factor is included in the model to account for the increasing resistance to motion that arises as an increasing ligand density reduces gap size in the ECM. Clearly, if ligand density becomes too large (the threshold may perhaps exceed densities ever realised in tissue), normal cell motion must cease. We set the threshold ligand concentration, L_{\max} , to be the concentration of binding ligands where the cell is no longer able to migrate through the matrix. As L approaches L_{\max} , the steric hindrance function diverges so that

$$\lim_{L \rightarrow L_{\max}} H(L) = \infty, \quad \lim_{L \rightarrow L_{\max}} \mathbf{v}(L) = \mathbf{0}.$$

If $L > L_{\max}$, we set $\mathbf{v}(L) = \mathbf{0}$. We discuss later how the model could be modified if future experiments were to show that motility persists at the largest possible ligand densities.

The traction force \mathbf{F}_{trac} at the cell-matrix interface is made up of opposing forward and backward components,

$$F_{\text{trac-f}} = F_{\text{R-L}} k n_f L, \quad F_{\text{trac-b}} = F_{\text{R-L}} k n_b L, \quad (3)$$

where $F_{\text{R-L}}$ is the force per ligand-integrin receptor complex and k is a binding constant. The magnitude of the traction force $F_{\text{trac}} = F_{\text{trac-f}} - F_{\text{trac-b}}$ simplifies to

$$F_{\text{trac}} = |\mathbf{F}_{\text{trac}}| = F_{\text{R-L}} k N (2\rho - 1) L, \quad (4)$$

where $\rho = n_f/N$ is the (constant) proportion of receptors on the front of the cell.

Substitution of Eq. (2) into Eq. (1) determines the cell speed $v(L)$ for a given cycle as

$$v(L) = |\mathbf{v}(L)| = |\mathbf{F}_{\text{trac}} + \mathbf{F}_{\text{prot}}| / (cH(L)). \quad (5)$$

In general, the alignment of the protrusion force \mathbf{F}_{prot} to the traction force \mathbf{F}_{trac} will vary from cycle to cycle in a random manner, so that the time-averaged velocity for a single cell, or the average velocity of an ensemble of cells moving in identical environments, must be computed by appropriate averaging of Eq. (5), as shown in “Appendix 1”.

In Table 1 we give representative values of model parameters; L_{\max} is the maximum ligand density in the absence of matrix degrading MMP activity, N_0 denotes the number of receptors in the absence of receptor increase due to MMP activity, and the parameter M_{\max} is discussed later. We write

$$F_{\text{trac}}^0 = F_{\text{R-L}} k N_0 L_{\max} (2\rho - 1), \quad (6)$$

and define a dimensionless parameter ε by

$$\varepsilon = \frac{F_{\text{prot}}}{F_{\text{trac}}^0}, \quad (7)$$

and so

$$\frac{F_{\text{prot}}}{F_{\text{trac}}} = \frac{\varepsilon N_0}{N}. \quad (8)$$

From the values given in Table 1, it is clear that $\varepsilon \ll 1$ [the value of ε ranges from 10^{-10} to 10^{-5}]. Unless the polarization of the cell is negligible (that is, $\rho \approx 0.5$) or the number N of integrin receptors on the cell is drastically reduced, the smallness of ε enables the effect of the protrusive force to be neglected and neither simulation nor careful mathematical averaging of the governing equations is required to predict mean cell speed over a cycle. We proceed for the moment on this assumption and speak of the cell speed rather than the mean cell speed in this case. “Appendix 1” details how slightly more complicated but still compact analytical results for the mean cell speed remain available even if the system parameters can be sufficiently changed that ε is no longer very small and averaging over the direction of the protrusion force is required.

We non-dimensionalize the model using

$$\ell = \frac{L}{L_{\max}}, \quad h(\ell) = \frac{H(L)}{H_0}, \quad u(\ell) = \frac{cH_0 v(L)}{F_{\text{trac}}^0}, \quad (9)$$

where $H_0 = H(0) > 0$ is the value of steric hindrance when no ligands are present. This gives the dimensionless cell speed as

$$u(\ell) = \frac{F_{\text{trac}}}{h(\ell) F_{\text{trac}}^0} = \frac{\ell N}{h(\ell) N_0}. \quad (10)$$

No MMP Activity

We address first the case without MMP activity, so

$$u(\ell) = \ell/h(\ell). \quad (11)$$

Since $0 \leq \ell \leq 1$ and $h(\ell)$ is an increasing function of ℓ which diverges to infinity as $\ell \rightarrow 1$, we have $u(\ell) \rightarrow 0$ as $\ell \rightarrow 1$ while as $h(0) = 1$ we have $u(\ell) \rightarrow 0$ as $\ell \rightarrow 0$. Thus $u(\ell)$ must always attain a maximum in the interior of the interval $0 < \ell < 1$. Thus biphasic behavior is the norm when MMPs are absent, a prediction that is robust so long as $\varepsilon \ll 1$. Specific illustrations will be found below in the “Results” section.

Modeling MMP Activity

We now consider matrix degradation by proteolytic MMP activity, with particular reference to how this affects the cell speed, especially the magnitude and position of its local maximum. The MMP enzymes typically act to degrade the ECM at the front of the cell,³¹ which may reduce both traction and steric hindrance. There is also a complex relationship between cell integrin receptor concentration and MMP

TABLE 1. Order of magnitude estimates of model parameters.

| Parameter | Value | Units | Source |
|-------------------|-------------------------|-------------------|---|
| M_{\max} | 10^{-6} | M | Homandberg <i>et al.</i> , ¹⁴ Yebra <i>et al.</i> ³⁶ |
| L_{\max} | 10^{-5} | M | Berry and Larreta-Garde ⁴ |
| k | 10^8 | M^{-1} | Akiyama and Yamada, ¹ Akiyama <i>et al.</i> ² |
| N_0 | 10^5 to 10^7 | | Akiyama and Yamada, ¹ Akiyama <i>et al.</i> , ² Goodman <i>et al.</i> , ¹¹ |
| F_{R-L} | 10^{-12} | N | DiMilla <i>et al.</i> ⁷ |
| F_{prot} | 10^{-12} to 10^{-9} | N | Harris <i>et al.</i> , ¹³ James and Taylor ¹⁸ |
| η | 10^2 | Nsm^{-2} | Akiyama and Yamada, ¹ Akiyama <i>et al.</i> , ² Goodman <i>et al.</i> ¹¹ |
| $2\rho - 1$ | 0.9 | | Schmidt <i>et al.</i> ²⁶ |
| a | 10^{-5} | m | Trinkaus ³⁰ |

concentration.^{3,24} We explore these issues in our modeling approach by including three effects now to be described that will be reflected in appropriate changes to quantities appearing in the right-hand side of the key Eq. (10) for the scaled cell speed $u(\ell)$. We shall study the individual consequences of each of these effects, and also their interplay.

We assume the concentration M of MMPs is dependent on the global ligand density, and we write

$$M = M_{\max}m(L/L_{\max}) = M_{\max}m(\ell). \quad (12)$$

We make this assumption because it seems reasonable that an ECM with a higher global ligand density will promote MMP activity more so than an ECM with a lower ligand density. Furthermore, it is unclear whether MMPs used by migrating cells are produced by these cells themselves or recruited from surrounding cells. Therefore rather than having MMP concentration depend on the local density of ligands surrounding the migrating cell, we choose to have it depend on the global density of ligands. Similarly, there is good evidence that the ligands of proteolytically generated ECM fragments regulate MMP production.^{29,32} In their review on adhesion receptors and cell invasion, Ivaska and Heino¹⁷ argue that “Metalloproteinase expression in cells may change in response to altered integrin expression or altered ligand concentration”. The production of ECM fragments must necessarily depend on the density of the ECM and thus there is a relationship between global ECM ligand density and MMP production. Defining $m(\ell)$ makes the comparison between the cases with and without MMPs straightforward. Moreover, all extant experimental information on ligand concentration appears to be global, and the assumption of uniform ligand density is in accord with previous relevant studies.¹²

(a) Traction may be decreased by a reduction in local ligand concentration (that is, the scaled ligand concentration ℓ decreases), acting to reduce cell speed. We preserve the meaning of ℓ as the scaled ligand density in the matrix globally, and write the

local ligand density in the vicinity of the cell as $\ell\phi[m(\ell)]$ in the numerator of Eq. (10).

(b) Traction may be increased by MMPs promoting an increase in the integrin receptor density (that is, N/N_0 increases), acting to increase cell speed. We assume an increase in receptor density proportional to MMP concentration, that is,

$$N = N_0 + rM = N_0 + rM_{\max}m(\ell), \quad (13)$$

where r is a positive constant, giving

$$\frac{N}{N_0} = 1 + \delta m(\ell), \quad \delta = \frac{rM_{\max}}{N_0}. \quad (14)$$

Experimental evidence^{3,24} suggests that $r > 0$, corresponding to an increase in the total number of receptors when MMPs are present and a decrease in the total number of receptors when MMPs are inhibited. We have also assumed that ρ , the proportion of receptors at the front of the cell, is unaltered as the receptor density changes (as in Harjanto and Zaman¹²). If one wished to allow for changes in this proportion, the right-hand side of Eq. (15) would acquire the extra factor $(2\rho_0 - 1)/(2\rho - 1)$, where ρ_0 is the fraction of integrin receptors on the front of the cell in the absence of MMPs, and ρ is the corresponding fraction when MMPs are present.

(c) At a given ligand density, the presence of MMPs may affect the structural integrity of the matrix, reducing the steric hindrance (that is, $h(\ell)$ is changed), acting to increase cell speed. We replace $h(\ell)$ in the denominator of Eq. (10) by $h(\ell)\psi[m(\ell)]$.

Hence, in the presence of MMPs, our model gives for the scaled cell speed

$$u(\ell) = \frac{\ell\phi[m(\ell)]\{1 + \delta m(\ell)\}}{h(\ell)\psi[m(\ell)]}. \quad (15)$$

The three functions ϕ , ψ and m are dimensionless functions of dimensionless arguments, and the parameter δ is also dimensionless. The MMP-free case is obtained by setting $\delta = 0$ and $\phi(m) \equiv \psi(m) \equiv 1$.

RESULTS FOR SINGLE CELL MOTILITY

Consistent with the algorithms used in Harjanto and Zaman,¹² the functional forms chosen in our examples are given by

$$\begin{aligned} h(\ell) &= (1 - \ell)^{-1}, & m(\ell) &= \alpha\ell, \\ \phi(m) &= e^{-\beta m}, & \psi(m) &= e^{-\gamma m}, \end{aligned} \quad (16)$$

where α , β and γ are non-negative constants. However we note that as quantitative experimental evidence of MMP effects accumulates, if alternative functional forms are identified, they will be easy to insert into the general analysis that we have laid out. Note that the steric hindrance function $h(\ell)$ diverges at $\ell = 1$.

No MMP Activity

When there is no MMP action, then from Eq. (11) we have

$$u(\ell) = \ell(1 - \ell). \quad (17)$$

This relation between cell speed and ligand density is shown as the solid blue curve in Fig. 2. The maximum speed is attained at ligand density $\ell^* = 1/2$, and $u(\ell^*) = 1/4$.

With MMP Activity

We consider each of the three effects of MMPs incorporated in the model on their own, and then consider when they act in conjunction. A few mathematical details are contained in ‘‘Appendix 2’’, where it is proved that for the choice (16) there is always precisely one local maximum of $u(\ell)$ at a scaled ligand density ℓ^* , where $0 < \ell^* < 1$. All predictions of the model are summarized in Table 2. We always take $\alpha > 0$ so that MMPs are present and parameters β , γ and δ only ever appear in the combinations $\alpha\beta$, $\alpha\gamma$ and $\alpha\delta$. To examine each effect of MMP activity in isolation, we set two of these parameter combinations to zero and vary the other. In Fig. 2 the nonzero combination is assigned the value unity in each case, but the formulae and inset figures in Table 2 cover general values. The MMP-free case $\alpha = 0$ (so that $\alpha\beta = \alpha\gamma = \alpha\delta = 0$) is included for reference in Fig. 2 (solid blue curve), while in all other cases, $\alpha > 0$.

(a) Local ligand density reduction only: $\beta > 0$, $\gamma = \delta = 0$. In this case the speed is always maximized at a smaller ligand concentration when this effect of MMPs is present alone [see Table 2(a)], and the maximum speed is reduced. The case $\alpha\beta = 1$ is shown as the broken black curve in Fig. 2.

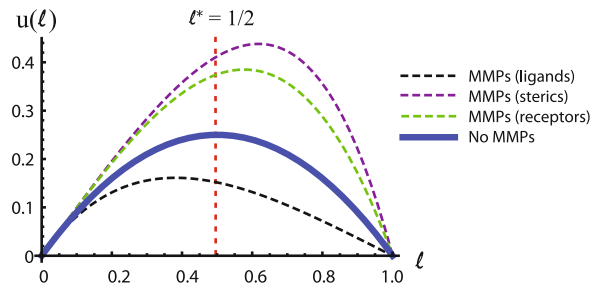


FIGURE 2. Dimensionless cell speed $u(\ell)$ as a function of dimensionless ligand concentration ℓ without MMPs (solid blue line) and with MMPs at scaled concentration $m(\ell) = \alpha\ell$ when they act to: modify ligand concentration/ECM (dashed black line, with $\phi(m) = e^{-\beta m}$); reduce steric hindrance (dashed purple line, with $\psi(m) = e^{-\gamma m}$); increase receptor number (dashed green line). The figure corresponds to the parameter values $\alpha\beta = 1$, $\alpha\gamma = 1$ and $\alpha\delta = 1$ in the limit $\epsilon \rightarrow 0$, but there is no visible difference over the range $0 \leq \epsilon < 0.01$ and the qualitative picture is the same for all positive values of α , β , γ and δ .

- (b) Steric hindrance reduction only: $\gamma > 0$, $\beta = \delta = 0$. In this case the speed is always maximized at a higher ligand concentration when this effect of MMPs is present alone [see Table 2(b)], and the maximum speed is increased. The case $\alpha\gamma = 1$ is shown as the broken purple curve in Fig. 2.
- (c) Integrin receptor increase only: $\delta > 0$, $\beta = \gamma = 0$. In this case the speed is always maximized at a higher ligand concentration when this effect of MMPs is present alone [see Table 2(c)], and the maximum speed is increased. The case $\alpha\delta = 1$ is shown as the broken green curve in Fig. 2.

We now consider the interplay between the three effects of MMP action incorporated in our model.

- (d) When both local ligand density reduction and steric hindrance reduction occur, we have competing opposite effects. For our illustrative choices of the functions $\phi(m)$ and $\psi(m)$, this competition is captured in the single parameter $\xi = \alpha(\beta - \gamma)$. When $\xi > 0$, the net effect is similar to local ligand density reduction alone, while if $\xi < 0$, the net effect is similar to steric hindrance reduction alone. The effect of the three mechanisms on the ligand concentration at which the cell speed is maximized is summarized in Table 2(d). In particular, we note that the curve $\xi = 2\alpha\delta/(2 + \alpha\delta)$ separates the parameter region where MMPs increase the ligand density ℓ^* at which maximal speed is attained above $1/2$ from the region where ℓ^* is decreased.

When multiple MMP effects are present, the effect on the value of the maximum cell speed $u(\ell^*)$, as well as the ligand density ℓ^* at which the maximum speed occurs, is of interest. Since $u(\ell^*)$ depends on both $\alpha\delta$ and $\xi = \alpha(\beta - \gamma)$, in Fig. 3 we show $u(\ell^*)$ when one of $\alpha\delta$ or $\xi = \alpha(\beta - \gamma)$ is held constant while the other is varied.

TABLE 2. The dimensionless ligand density ℓ^* at which the cell speed is maximal, illustrated for the steric hindrance function $h(\ell) = (1 - \ell)^{-1}$.

| MMP related functions | Exact formula for ℓ^* or equation for ℓ^* and limiting values | Plot of position of maximum ℓ^* |
|--|---|--------------------------------------|
| <p>(a) Only local ligand density reduction</p> <p>$\phi = e^{-\beta m}$ $\psi = 1, \delta = 0$</p> | $\ell^* = \frac{2 + \alpha\beta - \sqrt{(\alpha\beta)^2 + 4}}{2\alpha\beta}$ <p>$\ell^* < \frac{1}{2} \quad \lim_{\beta \rightarrow 0} \ell^* = \frac{1}{2} \quad \lim_{\beta \rightarrow \infty} \ell^* = 0$</p> | |
| <p>(b) Only steric hindrance reduction</p> <p>$\psi = e^{-\gamma m}$ $\phi = 1, \delta = 0$</p> | $\ell^* = \frac{\alpha\gamma - 2 + \sqrt{(\alpha\gamma)^2 + 4}}{2\alpha\gamma}$ <p>$\ell^* > \frac{1}{2} \quad \lim_{\gamma \rightarrow 0} \ell^* = \frac{1}{2} \quad \lim_{\gamma \rightarrow \infty} \ell^* = 1$</p> | |
| <p>(c) Only receptor density increase</p> <p>$\phi = 1$ $\psi = 1$ $\delta > 0$</p> | $\ell^* = \frac{\alpha\delta - 1 + \sqrt{1 + \alpha\delta + (\alpha\delta)^2}}{3\alpha\delta}$ <p>$\ell^* > \frac{1}{2} \quad \lim_{\delta \rightarrow 0} \ell^* = \frac{1}{2} \quad \lim_{\delta \rightarrow \infty} \ell^* = \frac{2}{3}$</p> | |
| <p>(d) All three MMP effects are present</p> <p>$\phi = e^{-\beta m}$ $\psi = e^{-\gamma m}$ $\xi = \alpha(\beta - \gamma)$ $\delta > 0$</p> | $\alpha\delta\xi\ell^3 + (\xi - \alpha\delta\xi - 3\alpha\delta)\ell^2 + (2\alpha\delta - 2 - \xi)\ell + 1 = 0$ <p>$\xi < \frac{2\alpha\delta}{2 + \alpha\delta} \Rightarrow \ell^* > \frac{1}{2}$ $\xi > \frac{2\alpha\delta}{2 + \alpha\delta} \Rightarrow \ell^* < \frac{1}{2}$</p> <p>$\lim_{\delta \rightarrow 0} \ell^* = \frac{2 + \xi - \sqrt{4 + \xi^2}}{2\xi}$ $\lim_{\delta \rightarrow \infty} \ell^* = \frac{3 + \xi - \sqrt{9 - 2\xi + \xi^2}}{2\xi}$</p> | |

When no MMP effects are present, $\ell^* = 1/2$. For MMP activity, α and at least one β, γ and δ are positive, but the other parameters may be zero. In parts (a)–(c) of the table, only a single MMP effect is present. In part (d) all three effects are present, but the parameters describing two of the effects can be combined under the single composite parameter $\xi = \alpha(\beta - \gamma)$. For this case, we show curves along which ℓ^* takes a constant value in parameter space.

Noting that in the MMP-free case where $\ell^* = 1/2$ and $u(\ell^*) = 1/4$, we are able to summarize the effect of changing any of the parameters α, β, γ and δ concisely in Fig. 4. There are three scenarios: ℓ^* moves left and $u(\ell^*)$ decreases; ℓ^* moves left and $u(\ell^*)$ increases (corresponding to the red shading); and ℓ^* moves right and $u(\ell^*)$ increases. In no case do we have ℓ^* moving right and $u(\ell^*)$ decreasing.

Although we have reported results for the case $\epsilon = 0$ and taken the MMP response to global ligand density to be given by $m(\ell) = \alpha\ell$, the picture is very similar at least up to $\epsilon \approx 0.1$, a value much higher than we are ever likely to encounter. Also, there is little sensitivity to changes in the functional form of $m(\ell)$ that preserve

its qualitative features (e.g., replacing $m(\ell) = \alpha\ell$ with $m(\ell) = e^{\alpha\ell} - 1$ where $0 < \alpha < 2$, although in this case there are four parameters that need to be considered rather than the two convenient combinations $\alpha\delta$ and $\xi = \alpha(\beta - \gamma)$, and a brief graphical summary such as Fig. 4 is no longer available.

Non-diverging Steric Hindrance

We have assumed above that steric hindrance, the resistance to cell movement through a 3D ECM matrix diverges to infinity as the ligand density increases to a critical value (L_{\max}), so that the cell is no longer able to move under these circumstances ($\mathbf{v} = \mathbf{0}$). This is a

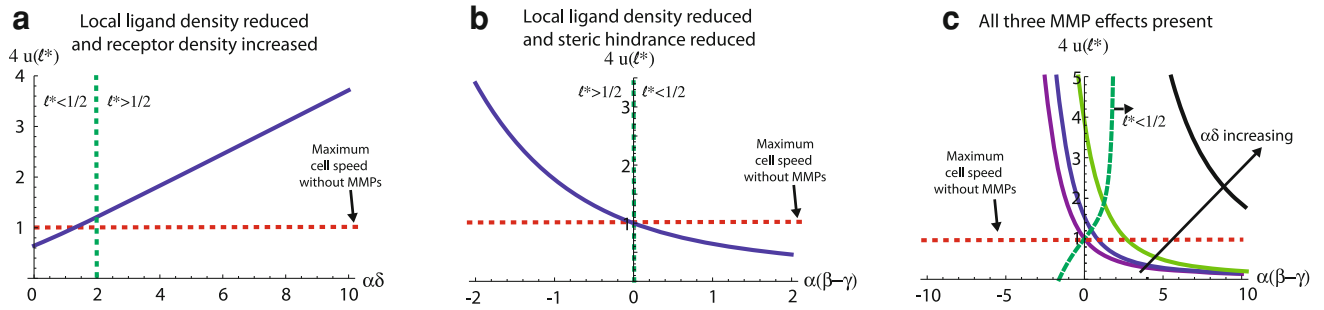


FIGURE 3. Maximum cell speed $u(\ell^*)$ when MMPs are present, for $h(\ell) = (1 - \ell)^{-1}$, $m(\ell) = \alpha\ell$, $\phi(m) = e^{-\beta m}$, $\psi(m) = e^{-\gamma m}$, and $\delta \geq 0$. (a) Varying the effect on receptor density ($0 < \alpha\delta < 10$) for a fixed level of local ligand density reduction ($\alpha\beta = 1$, $\gamma = 0$); (b) The competition between local ligand density reduction ($\beta > 0$) and steric hindrance reduction ($\gamma > 0$) with no receptor density increase ($\delta = 0$); (c) All three effects of MMPs present simultaneously: we show $u(\ell^*)$ as a function of $\xi = \alpha(\beta - \gamma)$ for the cases $\delta = 0$ (purple line), $\alpha\delta = 1$ (blue line), $\alpha\delta = 5$ (green line), $\alpha\delta = 100$ (black line). A plot of the solution when $\alpha\delta = 2\xi/(2 - \xi)$ and $\ell^* = 1/2$ is also shown (dashed green line).

reasonable assumption for cell migration through living tissue,^{6,38} but we consider briefly what the consequences of a bounded steric hindrance would be. At maximum ligand density the mean cell speed remains finite, but will it be biphasic? We continue to assume that the force ratio parameter ϵ is small enough to be taken as zero, although the formulae developed in “Appendix 1” enable the analysis to be extended to general values of ϵ if desired.

For the MMP-free case we see from Eq. (11) that the function $\ell/h(\ell)$ must be non-monotonic in the region $0 < \ell < 1$ in order for the mean cell speed to exhibit biphasic behavior. This places a restriction on the growth rate of $h(\ell)$. For example, if $h(\ell) = e^{\kappa\ell}$, where $\kappa > 0$, then the mean cell speed is biphasic if and only if $\kappa > 1$.

The MMP case is similar but a more complex restriction is placed on $h(\ell)$. If we use the bounded steric hindrance function $h(\ell) = e^{\kappa\ell}$ with our previous model ($m(\ell) = \alpha\ell$, $\phi(m) = e^{-\beta m}$, $\psi(m) = e^{-\gamma m}$, and δ as defined previously), and write $\xi = \alpha(\beta - \gamma)$ as before, then if the velocity is to be biphasic, we need to be able to satisfy the equation $(\xi + \kappa)\ell(1 + \alpha\delta\ell) = 1 + 2\alpha\delta\ell$ for $\ell = \ell^*$, where $0 < \ell^* < 1$. It is easy to show that no such solution is possible if $\xi + \kappa < (1 + 2\alpha\delta)/(1 + \alpha\delta)$. This suggests that a sufficiently rapid increase in steric hindrance as ligand density increases is important if biphasic cell speed behavior is to arise.

Time Dependent Model

Our approach has determined an analytical formula for the mean cell speed as a function of ligand concentration, which exhibits biphasic behavior and is particularly simple in the case when the parameter ϵ defined in Eq. (7) is small. Zaman *et al.*³⁷ and Harjanto and Zaman¹² determined mean cell speeds using a numerical approach. However, their approach is conceptually different to ours. Rather than considering the

speed $v(L)$ of a cell migrating through ECMs with different ligand concentrations L , they consider the speed of a cell migrating through one ECM that is degrading with time t . We compare our analytic formulae with the numerical work for the time-dependent description.

In the time-dependent formulation used for the previous simulations,^{12,37} Eqs (1)–(5) are used to determine the speed over a single time step and the protrusion direction is varied at random from step to step. The steric hindrance effect embodied in $H(L)$ (and $h(\ell)$ in the scaled model) was used in the simulations but this was not made clear in those papers. At the end of each time step in the simulation, the ligand density is changed and the simulation can be interpreted in two ways. If the physical circumstances correspond to a matrix whose global properties change with time—for example, if the motile cell concentration is appreciable and if MMPs diffuse significantly through the matrix, then the simulation corresponds to the history of a cell moving through an evolving matrix. Alternatively, time can be viewed simply as an artificial parameter that enables curves in physical parameter space to be varied.

It has been noted above that unless the force ratio parameter ϵ defined by Eq. (7) is allowed to be somewhat larger than is usually biologically relevant (for example by making the cell polarity very small), or the ligand density becomes many orders of magnitude smaller than its maximum value, the effects of the random direction changes on speed are small. However, in the time-dependent simulations, the ligand density used is $L(t) = L_{\max} - C_1 t$ and the simulation is run for $0 \leq t < L_{\max}/C_1$, so that in the late stages of the simulation, the approximation based on setting $\epsilon = 0$ becomes inappropriate. In that case, the full analysis outlined in “Appendix 1” becomes necessary and we have used that in comparing analytical results from our approach with simulations in the manner of

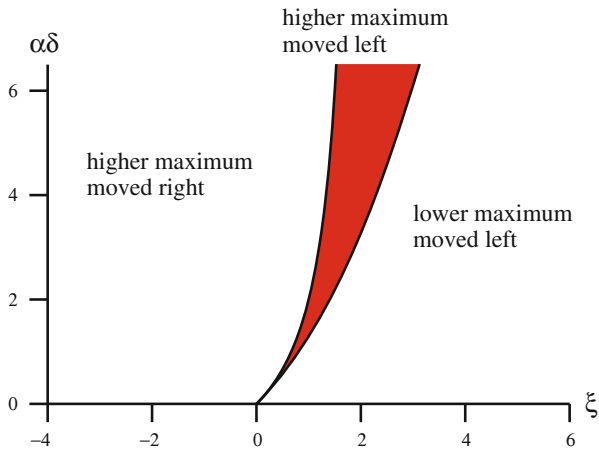


FIGURE 4. Consequences of all three MMP effects, for all parameters α , β , γ , δ varying, writing $\xi = \alpha(\beta - \gamma)$. The red region corresponds to the case when the maximum speed $u(\ell)$ increases over the MMP-free case [$u(\ell) > 1/4$], and is achieved at a lower ligand density ($\ell < 1/2$). The left boundary of the red region is given by $\xi = 2\alpha\delta/(2 + \alpha\delta)$. To the left of the red region, $\ell > 1/2$ and $u(\ell) > 1/4$, while to the right of the red region, $\ell < 1/2$ and $u(\ell) < 1/4$.

the earlier work. The steric hindrance function used is $H(t) = C_2/|L_{\max} - L(t)|$.

A comparison of simulations and analytical results (with and without MMP activity) is shown in Fig. 5. The simulations were rerun to produce this figure using MATLAB code from the earlier studies.^{12,37} Cell speed is plotted as a function of the instantaneous ligand density $L(t)$, so that all curves touch the axis on the right at maximal ligand concentration, corresponding to time $t = 0$, and on the left at a much reduced ligand concentration, corresponding to the end of the simulation run. At any instant, of course, the results of the time-dependent model simulations should match exactly with the analytical approach with all system attributes assigned their instantaneous values. For the case without MMP activity, setting up the exact correspondence between the analytic and simulation parameters is straightforward and results are shown in Fig. 5 (red curve—analytic results, blue stars—average over 100 simulations). Our analytical results are an excellent match for the simulation-based data. We explored other parameter values, and similar quality agreement is obtained.

MMPs are introduced into a time dependent model¹² using the same framework as in Zaman *et al.*,³⁷ using an MMP concentration $M(t)$ that is a prescribed function of t . Harjanto and Zaman¹² assume that MMPs act to increase the number of cell receptors and increase the rate of decay of ligand concentration. This corresponds with our previous model where $\phi < 1$, $\delta > 0$ and $\psi = 1$. They use a different increasing relationship between the number

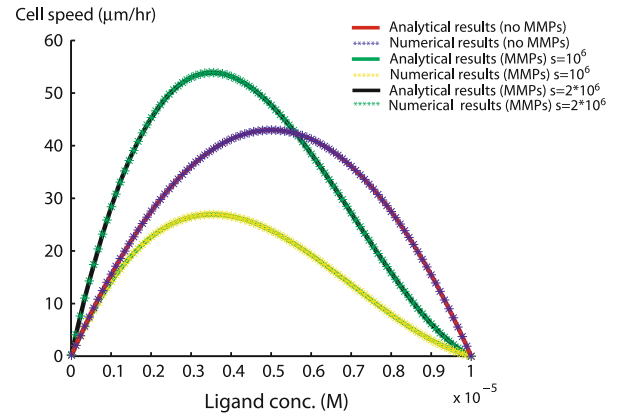


FIGURE 5. Comparison of averages over 100 simulations (shown as stars) and analytical results (shown as solid curves) for the mean cell speed with MMPs (green line and yellow stars, black line and green stars) and without MMPs (red line and blue stars) when ligand concentration is varied three orders of magnitude from 10^{-5} to 10^{-8} M. In this figure, as in Harjanto and Zaman,¹² the constant c in Eq. (2) is assigned a value by assuming low-Reynolds number viscous flow about a spherical cell ($c = 6\pi\eta a$). Parameter values: $F_{\text{progt}} = 10^{-9}$ N, $F_{\text{R-L}} = 10^{-12}$ N, $N = 10^7$, $k = 10^8$ M⁻¹, $\eta = 100$ Ns m⁻², $a = 10^{-6}$ m, $L_{\max} = 10^{-5}$ M, $\rho = 0.95$, $C_1 = 0.999/91 \times 10^{-5}$ M, $C_2 = 10^3$ M; when no MMPs are present, $C_3 = 1$ M and $C_4 = 0$; when MMPs act, $C_3 = 10^{-7}$ M, $C_4 = 9/91 \times 10^{-7}$ M, $C_5 = 10^2$ M⁻¹, and $s = 10^6$ M⁻¹ (green line and yellow stars), $s = 2 \times 10^6$ M⁻¹ (black line and green stars), $0 \leq t \leq 91$.

of cell receptors and the MMP concentration from our Eq. (13), namely

$$N(t) = N \times sM(t) = n_f(t) + n_b(t). \quad (18)$$

Ligand density reduction is incorporated by writing

$$F = F_{\text{R-L}}k(2\rho - 1)N(t)\phi[M(t)]L(t), \quad (19)$$

where $\phi[M(t)]$ is a decreasing function of time. To compare the numerical results in Harjanto and Zaman¹² with our analytic formulation, we need to recalculate the mean cell speed for a cell migrating in a degrading ECM using Eq. (20) from “Appendix 1”, and insert the functions

$$L(t) = L_{\max} - C_1t, \quad H(t) = C_2/|L_{\max} - L(t)|, \\ M(t) = C_3 + C_4t, \quad \phi[M(t)] = \exp[-C_5M(t)],$$

with appropriate values of the constants C_1, \dots, C_5 . These values, and the values of other parameters used are given in the caption to Fig. 5. Two different values of the parameter s defined by Eq. (18) are used and in each case we see biphasic cell speed behavior and the match between simulation and analytically derived results is excellent. The magnitude of the maximum speed and the position it is attained depends on the value of s , as one would expect from our previous analysis. When $s = 10^6$ M⁻¹, the maximum value achieved is lower and when $s = 2 \times 10^6$ M⁻¹, the maximum value achieved is higher. In the latter case,

receptor increase is sufficiently larger than traction reduction so that the maximum value of the mean cell speed is higher than the case without MMPs. When this is not the case ($s = 10^6 \text{ M}^{-1}$) then traction reduction causes the maximum value of the mean cell speed to drop compared to the case without MMPs.

DISCUSSION

We have presented a simple force balance model of a single cell in a single time-averaged cell motility cycle involving protrusion, adhesion and detachment, assuming that cell speed is a function of ECM ligand density. We were able to determine analytically the expected value of cell speed which is biphasic in ligand concentration and have shown that our model predicts the numerical results of previous computational models^{12,37} that have shown good agreement with *in vitro* experiments.^{8,19,23,35,38} Our model takes into account the cell's attachment to ligands in the ECM through receptors, the force generated from extending a protrusion into the ECM and the drag experienced by the cell. We also incorporated the resistance to cell movement due to the physical barrier of ligands, the steric hindrance, into the drag term so that the cell was unable to move once a threshold ligand concentration was obtained. We did not include signalling in our model, cell shape changes or the redistribution of receptors on the cell surface, and one could develop more complex models that incorporate these factors. However, by simply considering three biologically relevant effects of MMPs, we were able to reproduce the bimodal relationship of cell speed to ligand concentration and show that MMPs affect the value of the maximum in the mean cell speed and the optimal concentration of ligands.

We have determined analytical formulae for the expected value of cell speed when both MMPs are and are not present. This allows general statements in terms of parameters to be explored. In contrast, previous work was confined to numerical simulations, for specific parameter values. Our analytic approach generalizes and extends previous computational models that have shown good agreement with *in vitro* experiments. Our analysis has shown that when MMPs are present, the maximum mean cell speed will increase, compared to the case without MMPs, if MMPs act to increase cell receptors and or decrease steric hindrance. If MMPs act to reduce traction, then in combination with these other two mechanisms, the maximum value of the mean cell speed could decrease. If MMPs act solely to reduce traction then this will always be the case. Also we have shown that the value of ligand concentration where the maximum value of the mean cell speed can also change when MMPs are present.

Experiments in 3D where MMPs are inhibited³⁸ show a decrease in cell speed compared to the case when MMPs are not inhibited. It would be interesting to see whether the maximum of the mean cell speed shifts to higher or lower ligand concentrations when MMPs are inhibited. This could provide an opportunity to validate our model.

Our model makes use of the current state of knowledge for single cell migration and provides a convenient framework to analyse cell speed in complex environments. With recent developments in tissue engineering, novel biomaterial development and a multi-scale perspective of chronic wounds and cancer metastasis, understanding how cells operate in native-like environments is of paramount importance. For example, with our phenomenological model we can explore analytically the parameter regions where the effect of MMPs on cell speed bifurcates. This knowledge can be used in conjunction with future experimental results as a guide to gain some insight into the possible mechanisms which control proteolytic migration. An ability to characterize cellular migratory behavior through a rigorous analytic approach therefore has significant implications not only in understanding cellular function but also in creating tools to control and optimize cellular function and performance *in vitro* and *in vivo*.

APPENDIX 1

We show here how the computational models of previous studies^{12,37} can be given a precise mathematical formulation that enables the mean cell speed as a function of system parameters such as ligand density to be computed in terms of simple known functions, circumventing the need for simulation. The analytical formulae obtained require no restriction on the value of the force ratio parameter ϵ and the nature of the approximation in which the protrusion force is neglected is clearly revealed, demonstrating its innocence in the usual biologically relevant parameter regime.

In three-dimensions, we introduce Cartesian basis vectors $\hat{\mathbf{i}}, \hat{\mathbf{j}}$ and $\hat{\mathbf{k}}$, with $\hat{\mathbf{k}}$ in the direction of \mathbf{F}_{trac} , so $\mathbf{F}_{\text{trac}} = F_{\text{trac}} \hat{\mathbf{k}}$ and with $0 \leq \theta \leq \pi$ and $0 \leq \phi \leq 2\pi$,

$$\mathbf{F}_{\text{prot}} = F_{\text{prot}} \sin \theta (\cos \phi \hat{\mathbf{i}} + \sin \phi \hat{\mathbf{j}}) + F_{\text{prot}} \cos \theta \hat{\mathbf{k}}.$$

Since the integration element for isotropic random angles is $(4\pi)^{-1} \sin \theta d\theta d\phi$, the calculation of $\mathbb{E}\{|\mathbf{v}|\}$ as a double integral is straightforward and the final answer is

$$\mathbb{E}\{|\mathbf{v}|\} = \begin{cases} \frac{F_{\text{trac}}^2 + 3F_{\text{prot}}^2}{3H(L)cF_{\text{prot}}} & \text{if } F_{\text{prot}} > F_{\text{trac}}, \\ \frac{F_{\text{prot}}^2 + 3F_{\text{trac}}^2}{3H(L)cF_{\text{trac}}} & \text{if } F_{\text{trac}} > F_{\text{prot}}. \end{cases} \quad (20)$$

It may be noted that if we desired the probability density functions for $|v|$ rather than just their expected values, the problem is equivalent to a two-step Rayleigh random flight with unequal step lengths (see Hughes¹⁵ for details).

Any modeling of MMP activity that alters the values of one or more of F_{trac} , F_{prot} , or $H(L)$ can easily be accommodated in Eq. (20). As it will almost always be the case that $F_{\text{trac}} > F_{\text{prot}}$, we will usually have

$$\mathbb{E}\{|v|\} = \frac{F_{\text{prot}}^2 + 3F_{\text{trac}}^2}{3H(L)cF_{\text{trac}}} = \frac{F_{\text{trac}}}{H(L)c} \left[1 + \frac{1}{3} \left(\frac{F_{\text{prot}}}{F_{\text{trac}}} \right)^2 \right] \quad (21)$$

and often (as in case studies in the “Results” section), we have $F_{\text{prot}}/F_{\text{trac}} \ll 1$, leading to a further simplification. However, in our discussion of a time-evolving simulation approach^{12,37} in which the ligand density is very greatly reduced towards the end of the simulation time interval, we have used Eq. (20).

APPENDIX 2

We sketch the analysis of the location of the velocity maximum in Eq. (15) for the prescription (16) of the effects of MMPs. We have

$$u(\ell) = \ell(1 - \ell)(1 + \alpha\delta\ell) \exp[\alpha(\gamma - \beta)\ell],$$

so $u(0) = u(1) = 0$ and $u(\ell) > 0$ for $0 < \ell < 1$, ensuring that the continuous function $u(\ell)$ attains at least one local maximum inside the interval. Taking the natural logarithm and differentiating twice, we find that

$$\frac{u'(\ell)}{u(\ell)} = \frac{1}{\ell} + \frac{1}{\ell - 1} + \frac{\alpha\delta}{1 + \alpha\delta\ell} + \alpha(\gamma - \beta)$$

and

$$\frac{u''(\ell)}{u(\ell)} - \frac{u'(\ell)^2}{u(\ell)^2} = -\frac{1}{\ell^2} - \frac{1}{(\ell - 1)^2} - \frac{(\alpha\delta)^2}{(1 + \alpha\delta\ell)^2}.$$

We see that at relevant stationary points [i.e., $0 < \ell^* < 1$ and $u'(\ell^*) = 0$] we have $u''(\ell^*) < 0$, so there is always exactly one such stationary point, which is a both a local maximum and the global maximum of $u(\ell)$ for $0 \leq \ell \leq 1$. Its location is the unique solution in $0 < \ell < 1$ of the algebraic equation

$$\frac{1}{\ell} + \frac{1}{\ell - 1} + \frac{\alpha\delta}{1 + \alpha\delta\ell} + \alpha(\gamma - \beta) = 0. \quad (22)$$

If $\alpha\delta = 0$ or if $\alpha(\beta - \gamma) = 0$ the equation is quadratic and ℓ^* can be exhibited in simple form. In all other cases ℓ is given by solving a cubic equation, though we refrain from writing out the solution here. The limiting

behavior of the solution in any of the limits $\delta \rightarrow \infty$, $\alpha(\beta - \gamma) \rightarrow 0$ and $\alpha(\beta - \gamma) \rightarrow -\infty$ can easily be extracted from Eq. (22). Details will be found in Table 2.

Although for biological relevance one needs all of α , β , γ and δ to be non-negative, the conclusions we have just drawn concerning the maximum are true on the weaker assumption that $\alpha\delta > -1$ (which is needed to ensure that receptor density remains positive), with no restriction on the signs or magnitudes of α , β , γ or δ . Setting $\alpha = 0$ completely removes the effects of MMPs and leaves the speed maximal at $\ell = 1/2$, so in the analysis summarized in Table 2 we assume that $\alpha > 0$ and in some cases for brevity we write $\xi = \alpha(\beta - \gamma)$.

ACKNOWLEDGMENTS

This work is supported by the Australian Research Council (ARC). Kerry Landman is an ARC Professorial Fellow.

REFERENCES

- ¹Akiyama, S. K., and K. M. Yamada. The interaction of plasma fibronectin with fibroblastic cells in suspension. *J. Biol. Chem.* 260:4492–4500, 1985.
- ²Akiyama, S. K., E. Hasegawa, and K. M. Yamada. The interaction of fibronectin fragments with fibroblastic cells. *J. Biol. Chem.* 260:13256–13260, 1985.
- ³Baum, O., R. Hlushchuk, A. Forster, R. Greiner, P. Clézardin, Y. Zhao, V. Djonov, and G. Gruber. Increased invasive potential and up-regulation of MMP-2 in MDA-MB-231 breast cancer cells expressing the $\beta 3$ integrin subunit. *Int. J. Oncol.* 30:325–332, 2007.
- ⁴Berry, H., and V. Larreta-Garde. Oscillatory behavior of a simple kinetic model for proteolysis during cell invasion. *Biophys. J.* 77: 655–665, 1999.
- ⁵Borau, C., R. D. Kamm, and J. M. Garcia-Aznar. Mechano-sensing and cell migration: a 3D model approach. *Phys. Biol.* 8:066008, 2011.
- ⁶Burgess, B. T., J. L. Myles, and R. B. Dickinson. Quantitative analysis of adhesion-mediated cell migration in three-dimensional gels of RGD-grafted collagen. *Ann. Biomed. Eng.* 28:110–118, 2000.
- ⁷DiMilla, P. A., K. Barbee, and D. A. Lauffenburger. Mathematical model for the effects of adhesion and mechanics on cell migration speed. *Biophys. J.* 60:15–37, 1991.
- ⁸DiMilla, P. A., J. A. Stone, J. A. Quinn, S. M. Albelda, and D. A. Lauffenburger. Maximal migration of human smooth muscle cells on fibronectin and type IV collagen occurs at an intermediate attachment strength. *J. Cell Biol.* 122:729–737, 1993.
- ⁹Duband, J., S. Dufour, S. Yamada, K. Yamada, and J. Thiery. Neural crest cell locomotion induced by antibodies to $\beta 1$ integrins. A tool for studying the roles of substratum molecular avidity and density in migration. *J. Cell Sci.* 98(4):517–532, 1991.

- ¹⁰Friedl, P., Y. Hegerfeldt, and M. Tusch. Collective cell migration in morphogenesis and cancer. *Int. J. Dev. Biol.* 48:441–449, 2004.
- ¹¹Goodman, S. L., G. Risse, and K. von der Mark. The E8 subfragment of laminin promotes locomotion of myoblasts over extracellular matrix. *J. Cell Biol.* 109:799–809, 1989.
- ¹²Harjanto, D., and M. H. Zaman. Computational study of proteolysis-driven single cell migration in a three-dimensional matrix. *Ann. Biomed. Eng.* 38:1815–1825, 2010.
- ¹³Harris, A. K., P. Wild, and D. Stopak. Silicone rubber substrate: a new wrinkle in the study of cell locomotion. *Science* 208:177–179, 1980.
- ¹⁴Homandberg, G. A., F. Hui, C. Wen, C. Purple, K. Bewsey, H. Koepf, K. Huch, and A. Harris. Fibronectin-fragment-induced cartilage chondrolysis is associated with release of catabolic cytokines. *Biochem. J.* 321:751–757, 1997.
- ¹⁵Hughes, B. D. *Random Walks and Random Environments*, Vol. 1. Oxford, England: Oxford University Press, (1995).
- ¹⁶Huttenlocher, A., M. Ginsberg, and A. Horwitz. Modulation of cell migration by integrin-mediated cytoskeletal linkages and ligand-binding affinity. *J. Cell Biol.* 134(6):1551–1562, 1996.
- ¹⁷Ivaska, J., and J. Heino. Adhesion receptors and cell invasion: mechanisms of integrin-guided degradation of extracellular matrix. *Cell. Mol. Life. Sci.* 57:16–24, 2000.
- ¹⁸James, D. W., and J. F. Taylor. The stress developed by sheets of chick fibroblasts in vitro. *Exp. Cell Res.* 54:107–110, 1969.
- ¹⁹Keely, P. J., A. M. Fong, M. M. Zutter, and S. A. Santoro. Alteration of collagen-dependent adhesion, motility, and morphogenesis by the expression of antisense $\alpha 2$ integrin mRNA in mammary cells. *J. Cell Sci.* 108:595–607, 1995.
- ²⁰Lauffenburger, D. A. A simple model for the effects of receptor-mediated cell-substratum adhesion on cell migration. *Chem. Eng. Sci.* 44:1903–1914, 1989.
- ²¹Lauffenburger, D. A., and A. F. Horwitz. Cell migration: a physically integrated molecular process. *Cell* 84:359–369, 1996.
- ²²Lutolf, M. P., J. L. Lauer-Fields, H. G. Schmoekel, A. T. Metters, F. E. Weber, G. B. Fields, and J. A. Hubbell. Synthetic matrix metalloproteinase-sensitive hydrogels for the conduction of tissue regeneration: engineering cell-invasion characteristics. *Proc. Natl. Acad. Sci. USA* 100:5413–5418, 2003.
- ²³Palecek, S., J. C. Loftus, M. H. Ginsberg, D. A. Lauffenburger, and A. F. Horwitz. Integrin-ligand binding properties govern cell migration speed through cell-substratum adhesiveness. *Nature* 385:537–540, 1997.
- ²⁴Riikonen, T., J. Westermarck, L. Koivisto, A. Broberg, V. Kahari, and J. Heino. Integrin $\alpha 2\beta 1$ is a positive regulator of collagenase (MMP-1) and collagen $\alpha 1(I)$ gene expression. *J. Biol. Chem.* 270:13548–13552, 1995.
- ²⁵Schense, J., and J. Hubbell. Three-dimensional migration of neurites is mediated by adhesion site density and affinity. *J. Biol. Chem.* 275(10):6813–6818, 2000.
- ²⁶Schmidt, C., A. Horwitz, D. Lauffenburger, and M. Sheetz. Integrin-cytoskeletal interactions in migrating fibroblasts are dynamic, asymmetric, and regulated. *J. Cell Biol.* 123:977–991, 1993.
- ²⁷Schwartz, M. P., B. D. Fairbanks, R. E. Rogers, R. Rangarajan, M. H. Zaman, and K. S. Anseth. A synthetic strategy for mimicking the extracellular matrix provides new insight about tumor cell migration. *Integr. Biol.* 2:32–40, 2010.
- ²⁸Thiery, J. Epithelial-mesenchymal transitions in tumour progression. *Nat Rev. Cancer* 2:442–454, 2002.
- ²⁹Tremble, P., C. H. Damsky, and Z. Werb. Components of the nuclear signaling cascade that regulate collagenase gene expression in response to integrin-derived signals. *J. Cell Biol.* 129:1707–1720, 1995.
- ³⁰Trinkaus, J. P. *Cells Into Organs: The Forces That Shape the Embryo*. Englewood Cliffs, NJ: Prentice Hall, (1984).
- ³¹Verheijen, J. H., N. M. E. Nieuwenbroek, B. Beekman, R. Hanemaaijer, H. W. Verspaget, H. K. Ronday, and A. H. F. Bakker. Modified proenzymes as artificial substrates for proteolytic enzymes: colorimetric assay of bacterial collagenase and matrix metalloproteinase activity using modified pro-urokinase. *Biochem. J.* 323:603–609, 1997.
- ³²Werb, Z., P. M. Tremble, O. Behrendtsen, E. Crowley, and C. H. Damsky. Signal transduction through the fibronectin receptor induces collagenase and stromelysin gene expression. *J. Cell. Biol.* 109:877–889, 1989.
- ³³Wong, H. C., and W. C. Tang. Computational study of local and global ecm degradation and the effects on cell speed and cell-matrix tractions. *Nano Commun. Netw.* 2:119–124, 2011.
- ³⁴Wong, H. C., and W. C. Tang. Correlating simulation and experimental data of traction and cell speed as functions of substrate stiffness. In: *Proceedings of 2011 11th IEEE International Conference on Bioinformatics and Bioengineering, BIBE 2011*, 2011, pp. 240–244.
- ³⁵Wu, P., J. B. Hoying, S. K. Williams, B. A. Kozikowski, D. A. Lauffenburger. Integrin-binding peptide in solution inhibits or enhances endothelial cell migration, predictably from cell adhesion. *Ann. Biomed. Eng.* 22:144–152, 1994.
- ³⁶Yebrá, M., G. C. N. Parry, S. Stromblad, N. Mackman, S. Rosenberg, B. M. Mueller, and D. A. Cheresh. Requirement of receptor-bound urokinase-type plasminogen activator for integrin $\alpha v\beta 5$ -directed cell migration. *J. Biol. Chem.* 271:29393–29399, 1996.
- ³⁷Zaman, M. H., R. D. Kamm, P. Matsudaira, and D. A. Lauffenburger. Computational model for cell migration in three-dimensional matrices. *Biophys. J.* 89:1389–1397, 2005.
- ³⁸Zaman, M. H., L. M. Trapani, A. Sieminski, D. MacKellar, H. Gong, R. D. Kamm, A. Wells, D. A. Lauffenburger, and P. Matsudaira. Migration of tumor cells in 3D matrices is governed by matrix stiffness along with cell-matrix adhesion and proteolysis. *Proc. Natl. Acad. Sci. USA* 103:10889–10894, 2006.